Chemistry of Metals and Alloys

Chem. Met. Alloys 14 (2021) 31-37
Ivan Franko National University of Lviv
www.chemetal-journal.org

Structure and magnetic properties of the (Cr,*T*,Ni)$_4$Si phases, *T* = Fe, Ru, Pd

Romana-Iryna MARTYNIAK[1,2]*, Nataliya MUTS[1], Matej BOBNAR[3], Lev AKSELRUD[1,4], Roman GLADYSHEVSKII[1]

[1] *Department of Inorganic Chemistry, Ivan Franko National University of Lviv, Kyryla i Mefodiya St. 6, 79005 Lviv, Ukraine*
[2] *École Normale Supérieure, 45 rue d'Ulm, 75005 Paris, France*
[3] *Jožef Stefan Institute, Jamova Cesta 39, 1000 Ljubljana, Slovenia*
[4] *Max Planck Institut für Chemische Physik fester Stoffe, Nöthnitzer Straße 40, 01187 Dresden, Germany*
* *Corresponding author. E-mail: romana-iryna.martyniak@ens.psl.eu*

Received June 5, 2021; accepted December 29, 2021; available on-line April 1, 2022
https://doi.org/10.30970/cma14.0417

The π phase (Cr,*T*,Ni)$_4$Si, where *T* is Fe, Ru, or Pd, crystallizing with an Au$_4$Al-type structure (Pearson symbol *cP*20, space group *P*2$_1$3), was synthesized in three alloys of the Cr$_{26}$Fe$_9$Ni$_{47}$Si$_{18}$, Cr$_{26}$Ru$_9$Ni$_{47}$Si$_{18}$, and Cr$_{26}$Pd$_9$Ni$_{47}$Si$_{18}$ nominal compositions. The crystal structures of the (Cr,*T*,Ni)$_4$Si phases were refined from X-ray powder diffraction data: cell parameter *a* = 0.612574(9) nm for (Cr$_{0.32}$Fe$_{0.11}$Ni$_{0.57}$)$_4$Si; *a* = 0.614454(8) nm for (Cr$_{0.40}$Ru$_{0.08}$Ni$_{0.52}$)$_4$Si; *a* = 0.61831(1) nm for (Cr$_{0.33}$Pd$_{0.11}$Ni$_{0.56}$)$_4$Si. The temperature dependence of the magnetic susceptibility of the (Cr$_{0.40}$Ru$_{0.08}$Ni$_{0.52}$)$_4$Si compound was studied in external magnetic fields of up to 7 T and in the temperature range between 1.8 and 350 K. The Cr$_{26}$Ru$_9$Ni$_{47}$Si$_{18}$ alloy exhibits paramagnetic behavior governed by the modified Curie-Weiss law: $\chi_0 = 172.7 \cdot 10^{-6}$ emu g-at^{-1}; $C = 3.7 \cdot 10^{-3}$ emu g-at^{-1} K^{-1}; $\Theta_p = -34$ K.

X-ray powder diffraction / Crystal structure / βMn structure type family / Magnetic properties / Magnetic skyrmions

Introduction

Many of the most interesting solid-state phenomena occur in crystalline solids lacking an inversion symmetry. Recent advances in solid-state physics have led to the discovery of, among others, the topological Hall effect, high-temperature superconductivity and peculiar spin states. Magnetic skyrmions, an example of the latter, bear immense potential for immediate integration into daily-life technologies, particularly storage and logic devices.

Sustainability of data storage technologies is critical for further development of society in the information age. Modern information storage devices, relying on magnetic domain memory (RAM and DWM technologies), may soon be superseded by new and more efficient ways of storing and processing data. Incorporation of skyrmionic materials into daily-life application devices may begin a new era in the information handling.

Magnetic skyrmions are nanometer-size quasiparticles existing in magnetic materials with broken inversion symmetry. Due to their compact size and simplicity of nucleation and annihilation, they bear potential to one day become the ultimate information carriers [1]. The most potent prospective application of magnetic skyrmions in information technologies is the skyrmion racetrack memory [2]. Its principle is similar to that of the domain wall-based racetrack memory; however, in this case, the information is coded by a sequence of individual magnetic skyrmions. Such a novelty is advantageous as, in contrast to magnetic domains, magnetic skyrmions can be compressed (compared to unconstrained magnetic skyrmions), leading to a considerably higher density of data storage [3]. A further advantage of the skyrmion racetrack memory lays in its energy efficiency: magnetic skyrmions can move in the bulk of a magnet with a very low current density [4], what additionally proves the potential superiority of the skyrmion-based memory.

Skyrmion-based radiofrequency devices are another class of components for which the topological nature of magnetic skyrmions can be harnessed to introduce considerable improvements in nanoscale radiofrequency applications. For example, a dynamical mode associated with the topological nature of single skyrmions confined in magnetic dots

is the low-frequency breathing mode [5]. It has been proposed [6] that the skyrmion breathing mode induced by spin torques can be used to generate a radiofrequency signal if the dot that contains the skyrmion is part of a magnetoresistive device, such as a spin valve or a magnetic tunnel junction. One of the advantages of the resulting skyrmion-based spin torque oscillator, compared with, for example, a vortex-based spin torque oscillator, would be that the magnetic skyrmion, being a localized soliton, would be less sensitive to external perturbations and thus would display a more coherent dynamic [1].

Non-centrosymmetric ferromagnets bear high potential of hosting magnetic skyrmions, vortices, and bubbles. Magnetic skyrmions have already been observed in MnSi (structure type FeSi, Pearson symbol *cP*8, space group $P2_13$) [7-9], FeGe (structure type FeSi, Pearson symbol *cP*8, space group $P2_13$) [10], $Mo_3Fe_{1.5-x}Co_xRh_{0.5}N$ (structure type Mo_3Al_2C, Pearson symbol *cP*24, space group $P4_132$) [11], $Cu_2[SeO_3]O$ (structure type $Cu_2[SeO_3]O$, Pearson symbol *cP*56, space group $P2_13$) [12], $Co_{10}Zn_{10}$ (structure type βMn, Pearson symbol *cP*20, space group $P4_132$) and $Co_6Zn_8Mn_6$ (structure type βMn, Pearson symbol *cP*20, space group $P4_132$) [13], and Mo_3M_2N (*M* = Fe, Co, Ni, Rh) (structure type Mo_3Al_2C, Pearson symbol *cP*24, space group $P4_132$) [14]. Hence, taking into consideration the nature of currently known skyrmionic compounds, we decided to initiate our research in the Cr–Ni–Si system, since a careful review of the structural data has shown that the π phase in this ternary system crystallizes with a Au_4Al-type structure. The Au_4Al structure type is a substitution derivative of the βMn structure [15], which is already known to host magnetic skyrmions even at high temperatures [13].

This research is a continuation of our previous investigations [16-20], where we focused on the synthesis of compounds with chiral structures. Our previous results suggest that the magnetic properties of phases with Au_4Al-type structure (Pearson symbol *cP*20, space group $P2_13$ [12]) in the Cr–{Fe,Co,Cu,Pd}–Ni–Si systems are a function of isomorphic atom substitution. Having elucidated the effect of replacing 5 at.% of the Cr/Ni statistical mixture by Co in [17] and by Fe, Cu, and Pd atoms in [18], we now investigate the effect of replacing 9 at.% of Cr/Ni by Fe, Ru, and Pd atoms on magnetic characteristics of the alloys. The aim of this research work is to present the results of structural and magnetic investigations of $Cr_{26}Fe_9Ni_{47}Si_{18}$, $Cr_{26}Ru_9Ni_{47}Si_{18}$, and $Cr_{26}Pd_9Ni_{47}Si_{18}$ alloys.

Experimental

Samples of nominal composition $Cr_{26}Fe_9Ni_{47}Si_{18}$, $Cr_{26}Ru_9Ni_{47}Si_{18}$ and $Cr_{26}Pd_9Ni_{47}Si_{18}$ were prepared from high-purity elements (≥ 99.9 wt.%) by arc-melting in a water-cooled copper crucible with a tungsten electrode under an atmosphere of argon (99.998 vol.% Ar, which was additionally purified with a molten Ti getter) at $5\cdot10^4$ Pa pressure. Prior to establishing a constant-pressure Ar atmosphere for the synthesis, the furnace was cleaned with flowing Ar which was supplied at a pressure of $3\cdot10^4$ Pa. The alloys were annealed at 900°C under vacuum in an evacuated quartz ampoule in a VULKAN A-550 electric muffle furnace for 35 days and were cooled rapidly thereafter.

Phase analysis of the polycrystalline samples was based on the X-ray powder diffraction data recorded with a Huber Image Plate Camera – G670 diffractometer (Cu $K\alpha_1$ radiation, λ = 0.154056 nm). Crystal structure refinements were made with the Rietveld method using the program package FullProf Suite [21]. Crystallographic data on the structure types used for the refinements was taken from Pearson's Crystal Data – Crystal Structure Database for Inorganic Compounds [22]. TYPIX [15] was used to identify the structure types and standardize the structural parameters.

The elemental composition, qualitative and quantitative, of the samples was additionally verified using energy-dispersive X-ray spectroscopy (EDS). In order to determine the chemical composition of the crystalline phase, a scanning electron microscope (SEM) Tescan Vega 3 and AZtecLive real-time chemical imaging powered by an X-Max^N Silicon Drift Detector were employed.

The temperature dependence of magnetic susceptibility was measured on a SQUID magnetometer (MPMSXL7, Quantum Design) in external fields between 10 mT and 7 T and in the temperature range between 1.8 and 350 K.

Results and discussion

The $Cr_{26}Ru_9Ni_{47}Si_{18}$ and $Cr_{26}Pd_9Ni_{47}Si_{18}$ samples were investigated by EDS analysis. Integral EDS analysis of the alloy surfaces showed the following chemical compositions: $Cr_{31.11}Ru_{6.08}Ni_{41.93}Si_{20.08}$ and $Cr_{27.48}Pd_{8.85}Ni_{45.81}Si_{17.86}$. The $Cr_{26}Ru_9Ni_{47}Si_{18}$ sample was found to contain a single phase of the $Cr_{31.11}Ru_{6.08}Ni_{41.93}Si_{20.08}$ composition, whereas the $Cr_{26}Pd_9Ni_{47}Si_{18}$ alloy contained two phases: the $Cr_{26.75}Pd_{9.12}Ni_{45.93}Si_{18.19}$ matrix and $Cr_{30.90}Pd_{6.08}Ni_{53.45}Si_{9.57}$ grains belonging to a secondary phase.

X-ray powder diffraction patterns of the three investigated samples showed the presence of a crystalline phase with Au_4Al-type structure in the three alloys. However, the $Cr_{26}Fe_9Ni_{47}Si_{18}$ and $Cr_{26}Pd_9Ni_{47}Si_{18}$ samples also contained small amounts of a secondary phase, which was a (Ni,Cr,*T*,Si), *T* = Fe, Pd, solid solution (structure type Cu, Pearson symbol *cF*4, space group *Fm*-3*m*). The $Cr_{26}Ru_9Ni_{47}Si_{18}$ alloy contained a single phase with Au_4Al-type structure (Pearson symbol *cP*20,

space group $P2_13$). X-ray diffraction patterns of the polycrystalline samples $Cr_{26}Fe_9Ni_{47}Si_{18}$, $Cr_{26}Ru_9Ni_{47}Si_{18}$, and $Cr_{26}Pd_9Ni_{47}Si_{18}$ annealed at 900°C for 35 days are shown in Fig. 1, Fig. 2, and Fig. 3, respectively.

Details of the structural refinements on X-ray powder diffraction data obtained from the annealed $Cr_{26}Fe_9Ni_{47}Si_{18}$, $Cr_{26}Ru_9Ni_{47}Si_{18}$, and $Cr_{26}Pd_9Ni_{47}Si_{18}$ samples, together with the atomic coordinates and isotropic displacement parameters for the $(Cr_{0.32}Fe_{0.11}Ni_{0.57})_4Si$, $(Cr_{0.40}Ru_{0.08}Ni_{0.52})_4Si$, and $(Cr_{0.33}Pd_{0.11}Ni_{0.56})_4Si$ phases, are given in Table 1.

The $Cr_{26}Fe_9Ni_{47}Si_{18}$ sample was found to contain 93.7(4) wt.% of the $(Cr_{0.32}Fe_{0.11}Ni_{0.57})_4Si$ phase crystallizing with Au_4Al-type structure (Pearson symbol *cP*20, space group $P2_13$) and 6.3 wt.% of a secondary phase, which is a (Ni,Cr,Fe,Si) solid solution exhibiting the crystal structure of Cu (a = 0.356870(9) nm, *i.e.* close to values reported for the relatively broad solid solution of Cr in Ni).

The ratio of Cr, Fe, and Ni in the statistical mixture of atoms occupying the sites in Wyckoff positions 12*b* and 4*a* of the main phase was fixed in accordance with the nominal composition of the alloy and was not refined.

The $Cr_{26}Ru_9Ni_{47}Si_{18}$ sample contained a single $(Cr_{0.40}Ru_{0.08}Ni_{0.52})_4Si$ phase, crystallizing with a Au_4Al-type structure. The EDS analysis of this sample showed the following composition $Cr_{31(1)}Ru_{6.1(5)}Ni_{42(2)}Si_{20.9(8)}$.

The $Cr_{26}Pd_9Ni_{47}Si_{18}$ sample was investigated by X-ray diffraction and energy-dispersive X-ray spectroscopy. The two analyses indicated the presence of two crystalline phases in the alloy. The major phase, $(Cr_{0.33}Pd_{0.11}Ni_{0.56})_4Si$, was found to crystallize with the Au_4Al structure type and constitute 98.1(4) wt.% of the alloy. According to the EDS analysis, the composition of the main phase was $Cr_{26.7(5)}Pd_{9.1(1)}Ni_{46.0(1)}Si_{18.2(8)}$. The secondary phase (1.9(1) wt.%) of the alloy is a (Ni,Cr,Pd,Si) solid solution, crystallizing with a Cu-type structure (a = 0.35963(2) nm for $(Cr_{0.31}Pd_{0.06}Ni_{0.53}Si_{0.10})$). According to the results of the EDS investigation of the sample, the composition of the secondary phase is $Cr_{30.9(6)}Pd_{6.1(3)}Ni_{53.45(7)}Si_{9.6(7)}$.

Table 1 Details of the structural refinements on X-ray powder diffraction data for the $Cr_{26}Fe_9Ni_{47}Si_{18}$, $Cr_{26}Ru_9Ni_{47}Si_{18}$, and $Cr_{26}Pd_9Ni_{47}Si_{18}$ samples (annealed at 900°C for 35 days); $(Cr_{0.32}Fe_{0.11}Ni_{0.57})_4Si$, $(Cr_{0.40}Ru_{0.08}Ni_{0.52})_4Si$, and $(Cr_{0.33}Pd_{0.11}Ni_{0.56})_4Si$ phases with Au_4Al structure type (Pearson symbol *cP*20, space group $P2_13$).

Sample (nominal)	$Cr_{26}Fe_9Ni_{47}Si_{18}$	$Cr_{26}Ru_9Ni_{47}Si_{18}$	$Cr_{26}Pd_9Ni_{47}Si_{18}$
Phase	$(Cr_{0.32}Fe_{0.11}Ni_{0.57})_4Si$	$(Cr_{0.40}Ru_{0.08}Ni_{0.52})_4Si$	$(Cr_{0.33}Pd_{0.11}Ni_{0.56})_4Si$
Content [wt.%]	93.7(4) [a]	100	98.1(4) [b]
Cell parameter, a [nm]	0.612574(9)	0.614454(8)	0.61831(1)
V [nm^3]	0.229866(6)	0.231989(5)	0.236381(8)
Atomic coordinates	*M*1 in 12*b* x = 0.7953(2) y = 0.9533(2) z = 0.3768(3)	*M*1 in 12*b* x = 0.7961(2) y = 0.9522(2) z = 0.3754(3)	*M*1 in 12*b* x = 0.7931(2) y = 0.9518(2) z = 0.3799(2)
	*M*2 in 4*a* x = 0.6871(2)	*M*2 in 4*a* x = 0.6859(2)	*M*2 in 4*a* x = 0.6865(2)
	Si in 4*a* x = 0.0687(5)	Si in 4*a* x = 0.0672(4)	Si in 4*a* x = 0.0661(4)
Isotropic displacement parameters B_{ov} 10^{-2} [nm^2]	0.63(2)	0.52(1)	0.58(1)
Mixed sites, *M*1, *M*2	$Cr_{0.32}Fe_{0.11}Ni_{0.57}$	$Cr_{0.40}Ru_{0.08}Ni_{0.52}$	$Cr_{0.33}Pd_{0.11}Ni_{0.56}$
FWHM parameters: U V W	 0.043(3) -0.044(1) 0.030(1)	 0.058(2) -0.064(3) 0.0327(9)	 0.069(4) -0.029(5) 0.025(1)
Asymmetry parameter	0.129(3)	0.151(2)	0.129(3)
Density D_X [g cm^{-3}]	8.216	8.270	8.683
Radiation wavelength λ [nm]	Cu $K\alpha_1$, 0.154056		
Reliability factors R_B / R_F R_p / R_{wp} R_{exp} / χ^2	 2.88 / 8.06 1.22 / 1.84 1.01 / 1.84	 3.61 / 6.02 1.59 / 2.39 1.19 / 4.05	 4.43 / 5.01 2.04 / 2.99 1.22 / 5.97

[a] 6.3(1) wt.% additional phase (Ni,Cr,Pd,Si) solid solution with Cu-type structure; [b] 1.9(1) wt.% additional phase $(Cr_{0.31}Pd_{0.06}Ni_{0.53}Si_{0.10})$ with Cu-type structure, composition according to EDX analysis)

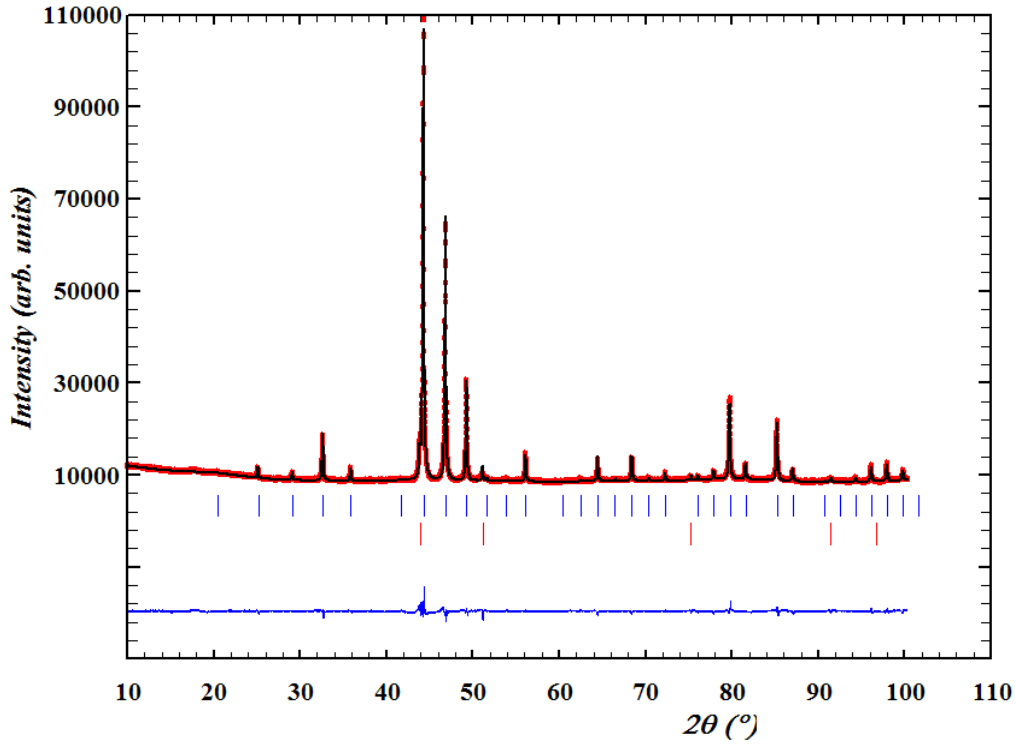

Fig. 1 Observed, calculated, and difference powder diffraction patterns of the $Cr_{26}Fe_9Ni_{47}Si_{18}$ sample (annealed at 900°C for 35 days); Cu $K\alpha_1$ radiation.

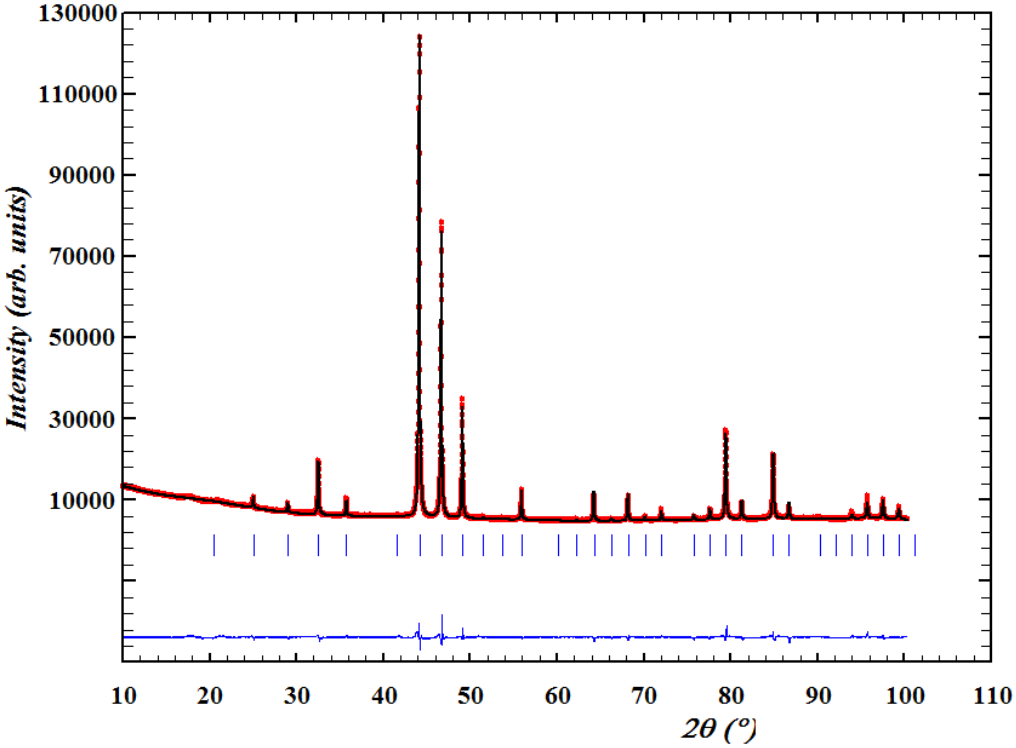

Fig. 2 Observed, calculated, and difference powder diffraction patterns of the $Cr_{26}Ru_9Ni_{47}Si_{18}$ sample (annealed at 900°C for 35 days); Cu $K\alpha_1$ radiation.

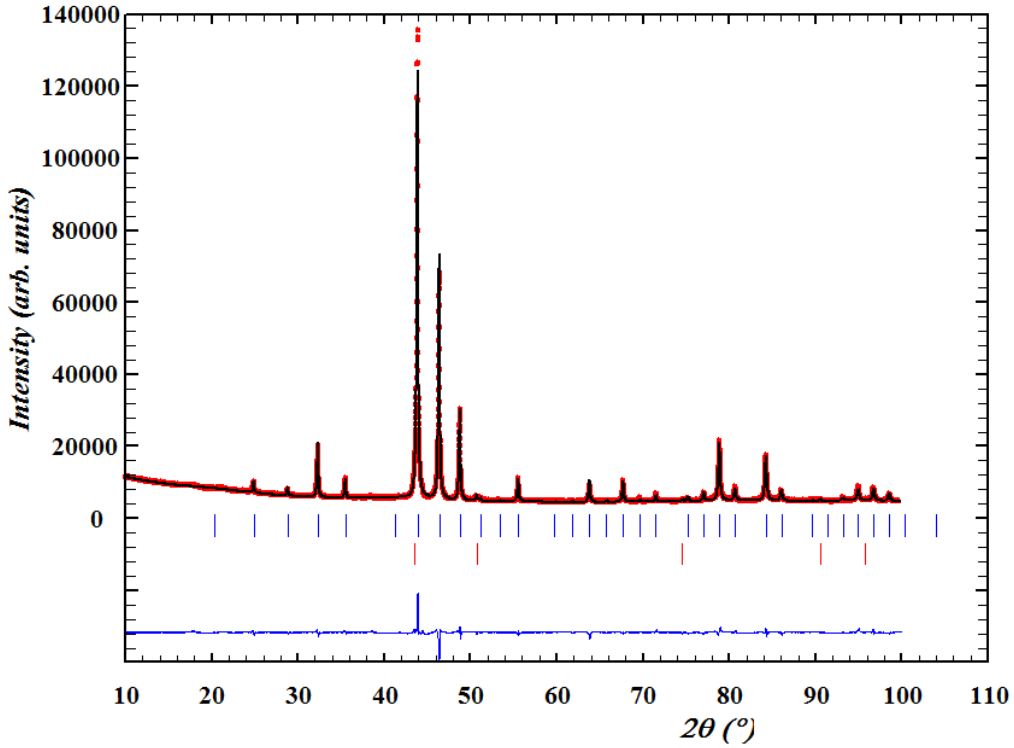

Fig. 3 Observed, calculated, and difference powder diffraction patterns of the $Cr_{26}Pd_9Ni_{47}Si_{18}$ sample (annealed at 900°C for 35 days); Cu $K\alpha_1$ radiation.

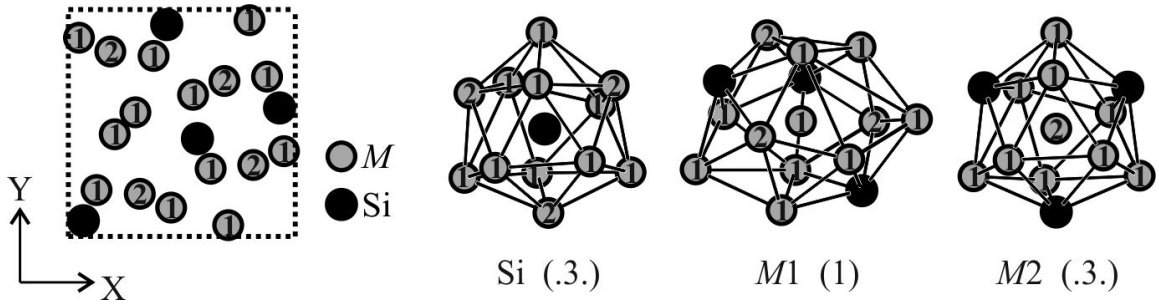

Fig. 4 Projection of the structure of $(Cr_{0.40}Ru_{0.08}Ni_{0.52})_4Si$ along [001] and coordination polyhedra of the three sites. *M*1, *M*2 are shown by grey circles, and Si as black circles. The site symmetries are indicated.

The cell parameter of the Au_4Al-type phase increases from a = 0.612574(9) nm for $(Cr_{0.32}Fe_{0.11}Ni_{0.57})_4Si$, through a = 0.614454(8) nm for $(Cr_{0.40}Ru_{0.08}Ni_{0.52})_4Si$, to a = 0.61831(1) nm for $(Cr_{0.33}Pd_{0.11}Ni_{0.56})_4Si$.

The Au_4Al structure type is a derivative of the βMn type. A projection of the structure of $(Cr_{0.40}Ru_{0.08}Ni_{0.52})_4Si$ along [001] is presented in Fig. 4. The sites in Wyckoff positions 12*b* and 4*a* are occupied by atoms of the statistical mixtures *M*1 and *M*2, respectively.

Nucleation of magnetic skyrmions in ferromagnets is possible if two conditions are fulfilled: a structural and a magnetic one. The structural condition of skyrmion stability lays in the absence of inversion symmetry in the crystal structure of the material, while the magnetic condition imposes the presence of ferromagnetic spin interactions [1]. The $(Cr_{0.40}Ru_{0.08}Ni_{0.52})_4Si$ phase, which adopts a Au_4Al-type structure, fulfills the structural condition for skyrmion nucleation, as it crystallizes in the non-centrosymmetric space group $P2_13$. It is worth mentioning that such a crystal structure bears high potential for carrying skyrmionic spin states, and compounds crystallizing with this space group have already been observed to host magnetic skyrmions at low temperature [4,7,10,13]. The structure type Au_4Al is an ordered substitution derivative of the βMn type,

where the 8-fold Mn position in βMn (Wyckoff position 8*c* in space group $P4_132$) is orderly occupied by Au and Al atoms (two sites in Wyckoff position 4*a* in space group $P2_13$), whereas the 12-fold Mn position (12*d*) is occupied exclusively by Au atoms (12*b*) [22,23]. Compounds crystallizing with structures belonging to the βMn structure type family exhibit high propensity to host peculiar spin states, including magnetic skyrmions [1,13].

In order to further investigate the potential of the $(Cr_{0.40}Ru_{0.08}Ni_{0.52})_4Si$ phase for hosting skyrmionic spin states, a series of magnetic measurements were conducted. Susceptibility measurements of the $Cr_{26}Ru_9Ni_{47}Si_{18}$ alloy in three magnetic fields (0.1, 3.5, and 7 T) revealed paramagnetic behavior. The susceptibilities of $Cr_{26}Ru_9Ni_{47}Si_{18}$ are field-independent at temperatures above approximately 25 K. Fig. 5 shows the data obtained at 3.5 T, which could be fit to a modified Curie-Weiss law $\chi = \chi_0 + C/(T - \Theta_p)$ above 20 K. The Curie-Weiss fitting of the experimental curve resulted in derivation of the following magnetic parameters for the $(Cr_{0.40}Ru_{0.08}Ni_{0.52})_4Si$ phase: $\chi_0 = 172.7 \cdot 10^{-6}$ emu g-at^{-1}, ($\chi_{dia} = -8.2 \cdot 10^{-6}$ emu g-at^{-1}; $\chi_{para} = 180.9 \cdot 10^{-6}$ emu g-at^{-1}), $C = 3.7 \cdot 10^{-3}$ emu g-at^{-1} K^{-1}, $\Theta_p = -34$ K, $N(E_F) = 5.6$ states eV^{-1} atom^{-1}. Here, χ_0 is the temperature-independent contribution to the susceptibility, C is the Curie constant and Θ_p is the paramagnetic Curie temperature. The negative diamagnetic susceptibility (χ_{dia}) was calculated for the Cr^{6+}, Pd^{4+}, Ru^{4+}, Ni^{2+}, and Si^{4+} ions [24] and was subtracted from χ_0 in order to obtain the positive Pauli paramagnetic contribution of the susceptibility (χ_{para}). The density of states at the Fermi level $N(E_F)$ was calculated from the value of χ_{para}.

The magnetic parameters obtained for the $Cr_{26}Ru_9Ni_{47}Si_{18}$ alloy suggest strong antiferromagnetic character of the interactions in this system. Consequently, the $(Cr_{0.40}Ru_{0.08}Ni_{0.52})_4Si$ phase does not present a suitable medium for nucleation of magnetic skyrmions. This fact makes the newly synthesized Ru-substituted compound less interesting for applications than other compounds previously obtained by isomorphic element substitution in the Cr–Ni–Si π-phase [18]. To achieve the desired magnetic properties, elements other than Ru should be incorporated into the alloys.

Conclusions

During the course of this research work, three π phases $(Cr_{0.32}Fe_{0.11}Ni_{0.57})_4Si$, $(Cr_{0.40}Ru_{0.08}Ni_{0.52})_4Si$, and $(Cr_{0.33}Pd_{0.11}Ni_{0.56})_4Si$, crystallizing with the Au_4Al-type structure, were synthesized. The newly synthesized compounds fulfill the structural condition for skyrmion nucleation, as they crystallize with the non-centrosymmetric space group $P2_13$. However, investigation of the magnetic properties of $(Cr_{0.40}Ru_{0.08}Ni_{0.52})_4Si$ showed that the compound is a paramagnet governed by a modified Curie-Weiss law, exhibiting rather strong antiferromagnetic interactions, inappropriate for skyrmions nucleation. A more conducive medium for skyrmion nucleation can possibly be created by replacing part of the atoms of the Cr/Ni statistical mixture in the π phase by elements other than Ru.

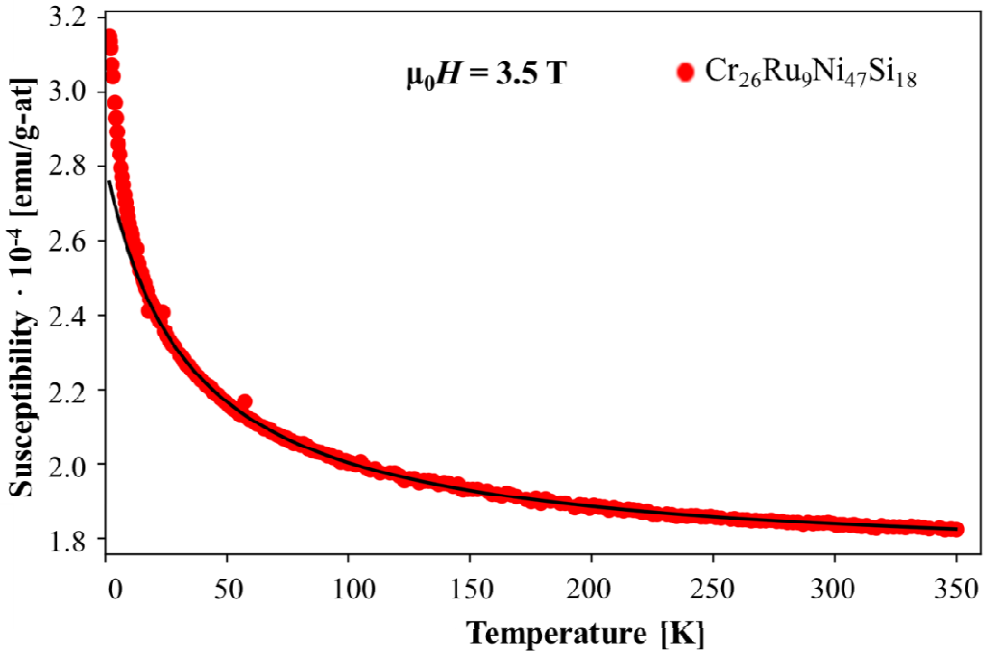

Fig. 5 Temperature dependence of magnetic susceptibility for the $Cr_{26}Ru_9Ni_{47}Si_{18}$ alloy measured in a 3.5 T magnetic field and fit to the modified Curie-Weiss law.

References

[1] A. Fert, N. Reyren, V. Cros, *Nat. Rev. Mater*. 2 (2017) 17031.

[2] W. Kang, Y. Huang, C. Zheng, W. Lv, N. Lei, Y. Zhang, X. Zhang, Y. Zhou, W. Zhao, *Sci. Rep*. 6, (2016) 23164.

[3] X. Zhang, G.P. Zhao, H. Fangohr, J.P. Liu, W.X. Xia, J. Xia, F.J. Morvan, *Sci. Rep*. 5, (2015) 7643.

[4] F. Jonietz, S. Mühlbauer, C. Pfleiderer, A. Neubauer, W. Münzer, A. Bauer, T. Adams, R. Georgii, P. Böni, R. A. Duine, K. Everschor, M. Garst, A. Rosch, *Science* 330 (2010) 1648-1651.

[5] J.-V. Kim, F. Garcia-Sanchez, J. Sampaio, C. Moreau-Luchaire, V. Cros, A. Fert, *Phys. Rev. B* 90, (2014) 064410.

[6] M. Carpentieri, R. Tomasello, R. Zivieri, G. Finocchio, *Sci. Rep.* 5 (2015) 16184.

[7] S. Mühlbauer, B. Binz, F. Jonietz, C. Pfleiderer, A. Rosch, A. Neubauer, R. Georgii, P. Böni, *Science* 323 (2009) 915-919.

[8] M. Ge, L. Zhang, D. Menzel, H. Han, C. Jin, C. Zhang, L. Pi, Yu. Zhang, *J. Alloys Compd.* 649 (2015) 46-49.

[9] M. Yamada, T. Goto, T. Kanomata, *J. Alloys Compd.* 364 (2004) 37-47.

[10] P. Pedrazzini, H. Wilhelm, D. Jaccard, T. Jarlborg, M. Schmidt, M. Hanfland, L. Akselrud, H. Q. Yuan, U. Schwarz, Yu. Grin, F. Steglich, *Phys. Rev. Lett.* 98 (2007) 047204.

[11] H. Hana, W. Wei, W. Liu, Y. Dai, H. Du, L. Pi, C. Zhang, L. Zhang, Yu. Zhang, *J. Alloys Compd*.739 (2018) 85–91.

[12] S.L. Zhang, A. Bauer, D.M. Burn, P. Milde, E. Neuber, L.M. Eng, H. Berger, C. Pfleiderer, G. van der Laan, T. Hesjedal, *Nano Lett.* 16(5) (2016) 3285-3291.

[13] Y. Tokunaga, X.Z. Yu, J.S. White, H.M. Rønnow, D. Morikawa, Y. Taguchi, Y. Tokura, *Nat. Commun*. 6 (2015) 7638.

[14] E. Haque, M. A. Hossain, *J. Alloys Compd.* 748 (2018) 117-126.

[15] E. Parthé, L. Gelato, B. Chabot, M. Penzo, K. Cenzual, R. Gladyshevskii, *TYPIX Standardized Data and Crystal Chemical Characterization of Inorganic Structure Types*, 4 vols., Springer Verlag, Berlin, 1993-4, electronic version 1996.

[16] R.-I. Martyniak, N. Muts, L. Akselrud, R. Gladyshevskii, *Visn. Lviv. Univ., Ser. Khim.* 59 (2018) 76-82 (in Ukrainian).

[17] R.-I. Martyniak, N. Muts, O. Sichevych, H. Borrmann, M. Bobnar, L. Akselrud, R. Gladyshevskii, *Solid State Phenom.* 289 (2019) 108-113.

[18] R.-I. Martyniak, N. Muts, M. Bobnar, L. Akselrud, R. Gladyshevskii, *Abstr. Int. Conf. Stud. Young Res. Theor. Exp. Phys. "HEUREKA-2019"*, Lviv, Ukraine, 2019, p. A14.

[19] R.-I. Martyniak, N. Muts, M. Bobnar, L. Akselrud, R. Gladyshevskii, *Coll. Abstr. XIV Int. Conf. Cryst. Chem. Intermet. Compd*., Lviv, Ukraine, 2019, p. 150.

[20] R.-I. Martyniak, N. Muts, A. Horyn, Ya. Tokaychuk, M. Bobnar, L. Akselrud, R. Gladyshevskii, *Visn. Lviv. Univ., Ser. Khim.* 61(1) (2020) 93-100.

[21] J. Rodriguez-Carvajal, *Commission on Powder Diffraction (IUCr) Newsletter* 26 (2001) 12-19.

[22] P. Villars, K. Cenzual (Eds.), *Pearson's Crystal Data – Crystal Structure Database for Inorganic Compounds*, Release 2018/19, ASM International, Materials Park (OH), 2019.

[23] E.I. Gladyshevskii, P.I. Kripyakevich, Yu.B. Kuzma, *J. Struct. Chem.* 3 (1962) 402-410.

[24] P.W. Selwood, *Magnetochemistry*, 2nd Ed., Interscience, New York, 1956, 435 p.